9 (2024) 100023

Contents lists available at ScienceDirect

IPEM-Translation

journal homepage: www.elsevier.com/locate/ipemt

Towards a locally constructed multi-element ultrasound imaging transducer for resource poor environments

A.J. Wilson [a,b,*], R.W. Taylor [b], S.E. Burrows [b], S.M. Dixon [b]

[a] Department of Research & Development, University Hospital, Coventry CV2 2DX, UK
[b] Department of Physics, University of Warwick, Coventry CV4 7AL, UK

ARTICLE INFO

Keywords:
Ultrasound
Random phased array
Construction

ABSTRACT

This paper investigates techniques and materials for making a multi-element ultrasound imaging transducer with craft-based techniques available in resource poor environments. The transducer housing can be conveniently divided into three parts: the body supporting the piezoelectric (PZT) elements and other components; the matching layer between the PZT elements and the human body; and the backing layer behind the PZT elements. Low-cost 3D printing systems based on photopolymers were found to be suitable for manufacturing the body. Finite Element Modelling (FEM) showed that the material characteristics of the backing layer and the thickness of the matching layer were much less critical than predicted by ultrasound plane wave theory and transmission line theory, respectively. The backing and matching layers are normally made from epoxy-tungsten composites that are pourable in the uncured state. However, the composite required for the backing layer was putty-like when uncured. When the tungsten was allowed to settle under gravity during curing, a 20 % by volume uncured tungsten-epoxy composite gave a 30 % by volume concentration of tungsten at the bottom when cured at 20–30 °C. These findings, when coupled with the findings from the FEM modelling, suggests that constructing a multi-element ultrasound imaging transducer using craft-based techniques is feasible.

1. Introduction

Whilst ultrasound imaging for healthcare in resource poor settings is desirable [1], making it widely available presents challenges including: the cost and robustness of equipment; the availability of parts and skilled personnel to maintain it; and skilled clinical personnel to use it [2]. The majority of medical ultrasound imaging is carried out using phased array transducers typically having up to 256 piezoceramic, commonly lead zirconate titanate (PZT), elements where the width and spacing are $<\lambda/2$ (typically <0.25 mm) to minimise grating lobes. Recent modelling work by one of the authors (AJW) has shown little difference in image quality when a sparse array 15-element ultrasound transducer with randomly arranged 2 mm diameter elements was compared to a 72-element phased array with $\lambda/2$ sized elements [3]. Transducers with elements $<\lambda/2$ require careful handling to avoid damage. In addition, the manufacture and repair of such arrays is costly, requiring specialist equipment and facilities not commonly found in resource poor environments. In contrast, sparse arrays of millimetre length scale elements can be manufactured and repaired using craft-based techniques where the skills and facilities are commonly available in resource poor settings.

The housing of a multi-element ultrasound transducer not only provides a way of mounting the elements but the design of the housing and the materials from which it is made determine the temporal performance of the transducer elements, including damping the natural resonance of PZT elements. The housing can be conveniently divided into three components:

- the 'body' which provides the mechanical support for the elements and other components;
- the 'matching layer' in front of the elements; and
- the 'backing layer' behind the elements.

In this paper we examine craft-based techniques for the manufacture of multi-element ultrasound imaging transducers in resource poor settings.

* Corresponding author at: Department of Research & Development, University Hospital, Coventry CV2 2DX, UK.
E-mail address: Adrian.Wilson3@nhs.net (A.J. Wilson).

https://doi.org/10.1016/j.ipemt.2024.100023
Received 12 December 2023; Received in revised form 9 February 2024; Accepted 13 February 2024
Available online 14 February 2024

2. Materials and Methods

2.1. The transducer body

For patient use, the outer surface of the body of the transducer must be water resistant and easily cleaned with alcohol and other disinfectant cleaners used in the clinical environment. One approach to making the transducer body is to machine this out of a hard plastic and acrylic has been successfully used in the past [4]. The advent of low cost (<5000€) widely available 3D printing systems potentially makes using these an attractive alternative to machining the body out of hard plastic. Two types of low cost 3D printing technology have been evaluated:

- a system that prints structures from acrylonitrile butadiene styrene (ABS) thermoplastic filaments laying down successive layers of a mesh of ABS strands (Upbox+; Beijing Tiertime Technology Co., Ltd., Beijing, P.R. China); and
- a system that prints proprietary photopolymer resins (FormLabs2; Formlabs Inc., Somerville, MA, USA).

For each system, the body to house the 2 mm-diameter, 15-element transducer used by Wilson [3] was constructed and evaluated against the criteria for patient use. Where these criteria were met, the density, ρ, and longitudinal velocity, v_l, of the printed material were measured and the acoustic impedance $z = \rho v_l$ calculated. The density was measured using an Archimedes balance.

2.2. The backing and matching layers

Traditionally, backing and matching layers have been made from epoxy composites containing tungsten and other particulates. Transmission line theory from communications engineering gives the thickness of the matching layer as $^{n\lambda}/_4$ where n is positive and odd to cancel out reflections from its surfaces and with an acoustic impedance, $Z_m = (Z_{pzt}\ Z_{tissue})^{½}$ to ensure maximum ultrasound intensity transfer to the tissue where Z_{pzt} is the acoustic impedance of the piezoelectric material and Z_{tissue} is the acoustic impedance of the tissue [5]. To minimise attenuation in the matching layer $n = 1$ is used. Plane wave theory predicts the thick backing layer should have an impedance, $Z_b = Z_{pzt}$ to prevent reflections at the backing layer-PZT interface and have attenuating properties so that reflections from its upper surface reaching the PZT do not contribute to the generated voltage resulting from reflections from within the tissue being imaged. It should be noted that these values of Z_m and Z_b are values from theory and not necessarily optimal values for a particular transducer in terms of its dynamic performance or sensitivity (e.g. Desilets et al. [6]), but rather represented a starting point for investigating materials.

The theoretical acoustic properties of the epoxy-composites were determined using an in-house implemented Mathematica™ (Wolfram Research Europe Ltd., Long Hanborough, UK) routine to numerically solve equations relating the composition of epoxy-tungsten composites to acoustic impedance [7]. The low viscosity epoxy Araldite 2020™ (Huntsman Advanced Materials (Switzerland) GmbH, Basel, Switzerland) was successfully used previously to make transducers as its low viscosity ensured minimal air bubbles after curing without preparing it under vacuum [4]. Using the solver routine with the measured properties of cured Araldite 2020 ($\rho = 1140$ kg m^{-3}, $v_l = 2522$ ms^{-1}, $Z = 2.88$ MPa sm^{-1}), the percentage of tungsten to give a matching layer with an acoustic impedance, $Z_m = (Z_{pzt}\ Z_{tissue})^{½}$, was found to be 20.4 % by volume (80.9 % by mass; Zm = 7.5 MPa sm^{-1}) and to give a backing layer with an acoustic impedance, $Z_b = Z_{pzt}$, was found to be 57.4 % by volume (95.7 % by mass; Zb = 33.7 MPa sm^{-1}).

2.2.1. Modelling

To investigate how the properties of the backing layer material and the thickness of the matching layer affected the temporal response of PZT elements to an acoustic drive, finite element method (FEM) modelling was used (PZFlex, OnScale, Atlanta, GA, USA). The circular-symmetric geometry is shown in Fig. 1 and the 2 mm diameter PZT element was resonant at 2.5 MHz. The acoustic impedance of the backing layer, Z_b was set to Z_{pzt}, the acoustic impedance of the matching layer, Z_m, to $(Z_{pzt}\ Z_{tissue})^{½}$ and water was used as the propagating medium. Matching and backing layer materials were modelled as 20.4 % and 57.4 % by volume tungsten-Araldite2020 composites, respectively. A 3-cycle 2.5 MHz, 1 MPa pressure drive was applied at the end of the water layer and the amplitude of the voltage generated by the PZT determined.

To investigate the effect of the thickness of the matching layer, the model geometry shown in Fig. 1 was used as the thickness was varied between zero and $^{5\ \lambda m}/_4$ in steps of $^{\lambda m}/_4$ where λ_m is the wavelength of ultrasound in the matching layer. The modelled voltages generated across the PZT for different thicknesses of matching layer were compared visually. A quantitative comparison was made using the full-width-half-maximum (FWHM) value of the waveform envelope determined by the fast Fourier transform (FFT) method.

To investigate how the acoustic impedance of the backing layer affected the temporal response of PZT elements to a pressure stimulus, the generated voltages across the PZT element were compared visually and using the FWHM value for the following backing layer materials: air; Araldite 2020; and 20.4 %, 38.6 % and 57.4 % by volume tungsten-Araldite2020 composites. The 38.6 % tungsten-Araldite2020 composite (91.2 % by mass, $Z = 13.4$ MPa sm^{-1}) was included because experimentally it was found to be the highest concentration of tungsten that gave a just pourable uncured composite. A $^{\lambda}/_4$ *thick* matching layer of *20.4 % tungsten in Araldite 2020 composite* was used for all backing layer simulations.

2.2.2. Measurement

All epoxy composites were made using Araldite 2020 and 25 μm tungsten powder (Goodfellow Goodfellow Cambridge Ltd, Huntingdon, UK). The equations relating the acoustic properties and composition of epoxy composites [7] gave the composition by volume. The required volumes were converted to masses using the density of components and the required quantities weighed before mixing. A rarely reported, but well recognised and common problem with epoxy composites is they fail to cure properly leaving the resultant material 'spongy' rather than hard.

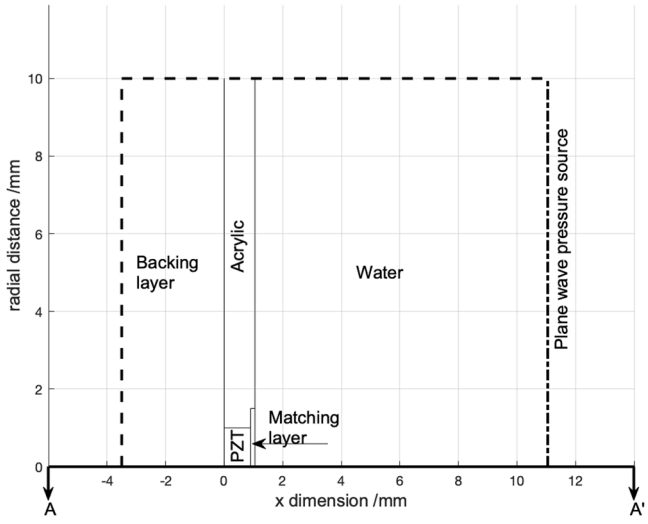

Fig. 1. A scale drawing of the geometry used for the axisymmetric 3d modelling which is rotationally symmetric about AA'. The thick dashed black lines are model boundaries implemented as 'perfectly matched layers' (PMLs). Internal material boundaries are shown as thin black lines. The 3-cycle plane pressure wave is applied to the boundary shown as a dot-dash line.

Different procedures for mixing and curing the epoxy, including the temperature at which both were performed were evaluated to determine the optimal one.

Initial experiments showed that: the uncured 57.4 % composite for the backing layer had the consistency of a thick putty; an uncured 38.6 % composite could be just poured but was too viscous to fill a 45 mm diameter mould without air gaps; but that an uncured 20.4 % tungsten-Araldite2020 composite could be readily mixed and poured into the mould without air gaps. Therefore, a different approach to producing a pourable composite for the backing layer was required. Tungsten is denser than Araldite 2020 and will fall under gravity during curing of the composite, accumulating at the bottom and resulting in a reducing percentage of tungsten with distance from the base. Reflections occur at discontinuities in acoustic impedance and acoustic impedance changes non-linearly but monotonically in tungsten-epoxy composites [7]. Therefore, if the change in the concentration of tungsten decreases smoothly with distance from the PZT there will be no discontinuities in acoustic impedance and no reflections. To investigate the potential of using this approach to create a backing layer, 20 % by volume uncured tungsten-Araldite2020 composites were poured into four tubular moulds approximately 27 mm long and 45 mm in diameter. Samples were cured at 10 °C, 20 °C, 30 °C and 40 °C in a temperature-controlled environment until solid. The resultant rods were sliced at 4.5 mm intervals along their length to create discs. The density of each disc was measured from which the volume fraction of tungsten was calculated and the acoustic impedance determined [7].

A transducer was made using a single element version of the transducer body shown in Fig. 2. The transducer had a 2 mm diameter 2 MHz PZT element (PRYY-0886, PI (Physik Instrumente) Ltd, Cranfield, UK), a $^{3}\,\lambda/_{4}$ thick, 20.4 % tungsten-Araldite2020 composite matching layer cured at 40 °C with the body held vertical with the matching layer uppermost and a 20 % by volume tungsten-Araldite2020 backing layer cured at 25 °C with the body held vertical with the top of the backing layer uppermost. The matching layer was poured and cured so it was of greater depth than required. Once cured the matching layer was polished back to the required thickness using wet-dry abrasive papers. The transducer was mounted vertically in a large water tank (600 mm x 600 mm) filled to a depth of approximately 80 mm with the PZT element 10 mm below the surface. A large 50 mm thick acrylic block was placed directly beneath the transducer on the bottom of the tank. The PZT element was driven by an 80 V, 500 ns wide pulse. The voltage generated across the PZT element resulting from ultrasound reflections from the block was recorded and the FWHM value determined.

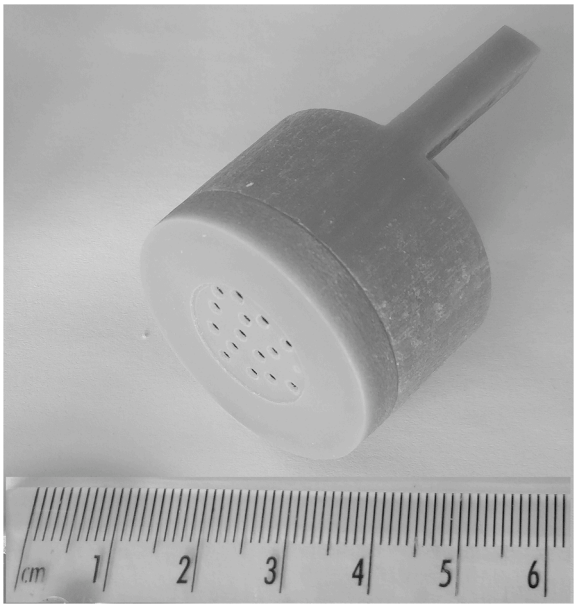

Fig. 2. A transducer body for the 15-element sparse random phased array transducer from [3] printed in a photopolymer resin.

3. Results

3.1. Transducer body

The transducer body 3D printed with ABS filament, even on the highest density setting, was found to allow water into the printed matrix and was unable to accurately print the surface structure to hold the PZT elements. Painting the surface with acetone considerably reduced the ingress of water into the matrix structure but was not 100 % effective at stopping it.

The transducer body 3D printed with photopolymer resin (Fig. 2) was watertight and could be wiped over with alcohol and disinfectant cleaning materials without problems and thus met the criteria for patient use. If left submerged in alcohol for periods of more than 1 h it did absorb some alcohol and its mass increased by 5 % after 12 h in isopropyl alcohol. The density of the material was measured to be 1179 kg m^{-3}, its longitudinal velocity was measured to be 2491ms^{-1} which gave an acoustic impedance of 2.93 MPa sm^{-1}.

3.2. The backing and matching layers

3.2.1. Modelling

A visual inspection of the PZT voltages generated as the thickness of the matching layer was increased (Fig. 3A) showed that there was little difference in the oscillatory behaviour of the element for matching layers with thicknesses between $^{\lambda m}/_{4}$ and λ_m. The lowest FWHM value was for $^{\lambda m}/_{4}$ but the differences with the other thicknesses modelled was small. Importantly, there was little difference in FWHM values between the odd and even multiples of $^{\lambda m}/_{4}$.

From Fig. 3B it can be seen that there are substantial post-excitation oscillations of the PZT with air which decreased when a backing layer was added. These oscillations appeared of lower amplitude with a longer cycle duration when tungsten-Aralide2020 composites were used as the backing layer with little difference in the amplitude of the oscillations as the percentage of tungsten in the composite increased. The low frequency components are the result of radial vibration modes. The FWHM values changed little as the percentage of tungsten was increased from zero to 38.6 %. The 57.4 % composite gave the largest FWHM value although the oscillations after the FWHM period appear of lower amplitude than for the other composites.

3.2.2. Measurement

Some of the early composites made were ‘spongy’ having failed to completely cure, a problem that increased with increasing tungsten. A substantial number of different approaches to mixing the composites were tried and a procedure for the 20.4 % composite was established where the two parts of the epoxy were mixed and stirred for 10 min at 30 °C before the tungsten powder was added slowly accompanied by thorough stirring. This was found to reliably produce composites that fully cured in typically 3 times the cure-time stated in the data sheet [8] and this procedure was used throughout.

The results for the tungsten concentration of different layers in the 20 % composite samples cured at different temperatures can be seen in Fig. 4. From Fig. 4A it can be seen that at 20 °C and 30 °C there was an approximately 50 % increase in the volume concentration of tungsten in the lowest layer with a corresponding decrease in the upper layers. Little difference is seen when the composite is cured at 10 °C and 40 °C. It should be noted that the low concentration of tungsten at 25 mm above the base for the sample cured at 10 °C is not accompanied by the large increase in the bottom-most layer as seen in the samples cured at 20 °C and 30 °C. Fig. 4B shows the calculated acoustic impedance for each measurement with an approximately 25 % increase in acoustic

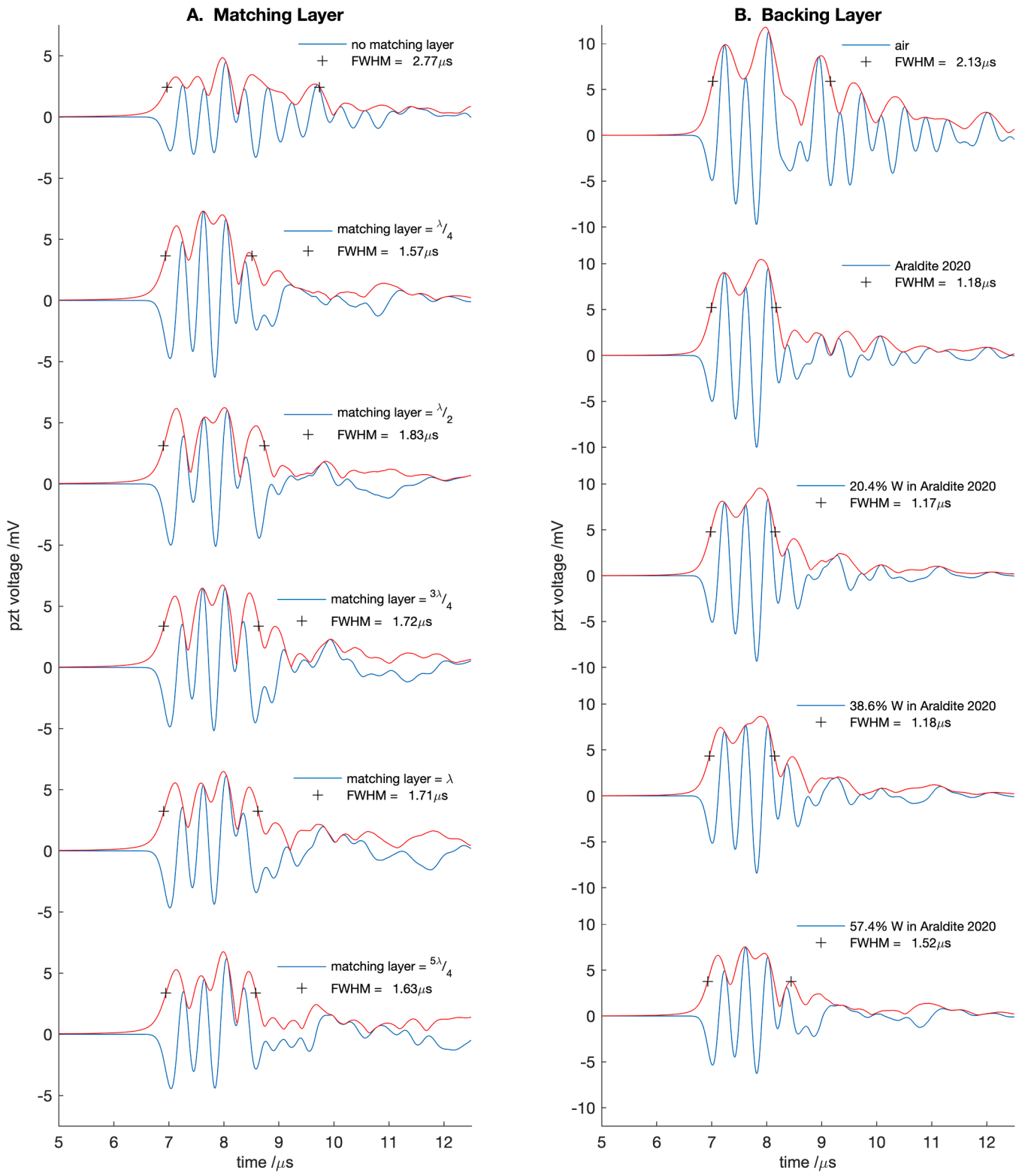

Fig. 3. Modelled time histories together with the envelope and FWHM value of the voltage across the PZT as: A the thickness of the 20.4 % tungsten in Araldite 2020 composite matching layer increases for a 3-cycle plane pressure wave applied through the water medium; and B, different backing layer materials were used where the matching layer was a $\lambda/4$ thick, 20.4 % tungsten (W) in Araldite 2020 composite. For each plot, the blue line shows the modelled PZT voltage, the red line is the waveform envelope determined by the FFT method and the FWHM points are marked '+'.

impedance in the lowest layer for samples cured at 20 °C and 30 °C.

An example of the signal recorded from the transducer placed above the acrylic block in the water tank is shown in Fig. 5. The shape and FWHM of the response are consistent with those seen from the simulations (Fig. 3).

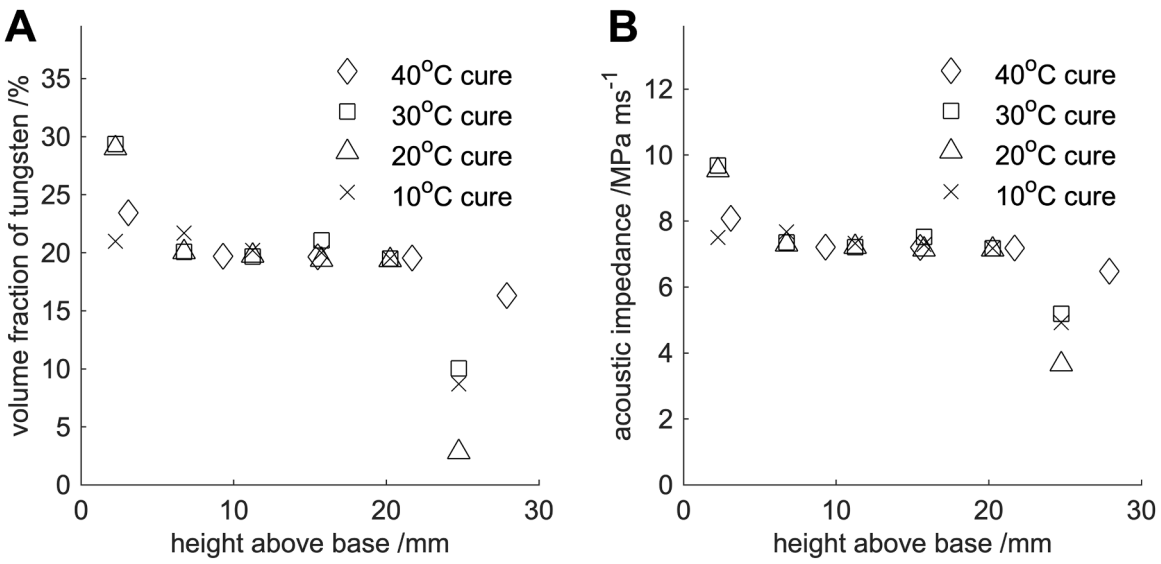

Fig. 4. Graphs showing the volume of tungsten (A) and acoustic impedance (B) in the different layers of the 20 % tungsten-Araldite2020 composite samples as the cure temperature is changed.

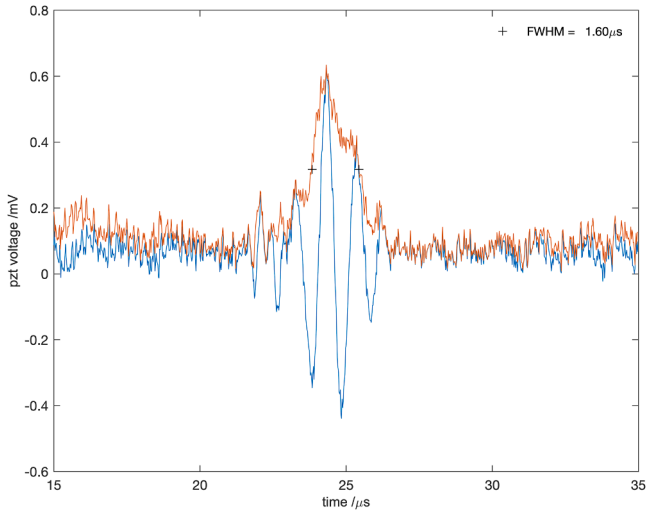

Fig. 5. Measured time history together with the envelope and FWHM value of the voltage across the PZT for the reflected ultrasound signal from an acrylic block approximately 20 mm away after the PZT was excited with an 500 ns 80 V pulse. The blue line shows the measured PZT voltage, the red line is the waveform envelope determined by the FFT method and the FWHM points are marked '+'.

4. Discussion and conclusions

The results show that 3D printing of the transducer body using ABS filaments is not viable whereas the 3D printing with photopolymer resins is. In addition to the water ingress, the material created during 3D printing with ABS filaments is mesh-like and would have anisotropic ultrasound properties at imaging frequencies. The measured density and acoustic impedance of the cured photopolymer resin is close to both acrylic, which has been used previously [4], and cured Araldite 2020. The modelling showed that the 3D printed photopolymers could not be used for the backing and matching layers. There are some limitations in using the photopolymer. Firstly, whilst the requirement is to be wiped over with alcohol-based cleaning products, the absorption of alcohol when soaked is undesirable in the clinical environment. Secondly, whilst the resolution of the current generation of photopolymer resin printers is typically quoted as 25μm this is in solid structures and creating sub-millimetre thick structures is unreliable. This makes creating small structures for accurately positioning the PZT elements in regions where there should be backing or matching layer material for transducer performance challenging. As an example, unpublished modelling results show that surrounding the PZT with matching layer material minimizes radial modes of vibration.

The theory that predicts the thickness and acoustic impedance of the matching layer has its origins in lumped parameter transmission line models whilst the acoustic impedance of the backing layer comes from ultrasound plane wave theory. FEM, which models spatial propagation of ultrasound in the transducer components and non-piston like modes of vibration in the PZT [4], suggest that both the thickness of the matching layer and composition of the backing layer are much less critical than predicted by these theories for transducers using millimetre length scale elements. This supports the use of craft-based techniques to build multi-element imaging transducers using such elements. Craft-based construction is still challenging: the $^{3\lambda}/_{4}$ matching layer of the 2 MHz single element transducer tested was 0.6 mm thick. Hand soldered or glued electrical connections to the PZT can be 0.5 mm thick unless great care is taken.

A robust procedure was established for reliably producing fully cured composites that were hard and therefore could be cut, machined and polished. However, it is worth noting that the time to produce fully cured samples was much longer than the times given in the data sheet for Araldite 2020 [8].

The uncured epoxy composites need to be liquid so they can be poured into the body to form well bonded interfaces without leaving air-pockets. The 20.4 % by volume epoxy-tungsten composite required for the matching layer fulfils this requirement whilst neither the 38.6 % nor 57.4 % by volume epoxy-tungsten composite met that requirement. The approach of allowing the tungsten to settle under gravity whilst curing at between 20 °C and 30 °C gives a way of creating a pourable backing layer with sufficient density next to the PZT to give an appropriate dynamic performance. Conversely, curing the composites at either 10 °C or 40 °C gave the homogeneous material required for the matching layer. Any material with a lower fraction of tungsten at the outer surface of the matching layer (see Fig. 4) is removed during polishing.

From Stokes Law it can be shown that the velocity of particles, v, settling under gravity in a viscous liquid is given by [9]:

$$v = \frac{2}{9}\left(\frac{\rho_p - \rho_f}{\mu}\right) g r^2 \quad ((1))$$

where ρ_p is the density of the particle material, ρ_f is the density of the fluid, μ is the viscosity of the fluid, g is the acceleration due to gravity and r is the radius of the particles. The published density of uncured Araldite 2020 [8] and the measured density of the cured epoxy are similar, but unfortunately there is no data for the viscosity of Araldite 2020 during curing, so theoretical prediction of the concentration of tungsten with depth as the powder settled under gravity was not possible. The cure time decreases with increasing temperature [8] as does the duration of the liquid phase and hence the period during which the tungsten can move. During the liquid phase the velocity of the powder particles is inversely proportional to viscosity (Eq. (1)) and the viscosity reduces with increasing temperature. In addition, the cure process is exothermic and hence the change in viscosity with time will be non-linear. These complex changes during curing mean that for a cure temperature of 40 °C the movement of the tungsten powder particles is minimal whilst at 30 °C and 20 °C there is substantial movement giving the increased tungsten concentration at the lowest level (Fig. 5A). At 10 °C the cure time is the longest but it would appear the viscosity is high due to the low temperature resulting in a low velocity of movement (Eq. (1)) and hence less overall movement of the tungsten powder. The 10 °C sample was the hardest to make and cure. The apparent loss of tungsten in this sample could be due to poor binding of the particles in the composite resulting in loss of tungsten from the cut surfaces. However, the shape is consistent with reduced particulate movement. Increasing the particle size increases the velocity, but the particle size must be very much less than the wavelength of the ultrasound to achieve the Rayleigh scattering to maximise attenuation. Although the modelling work described in this paper and in [3] used a frequency of 2.5 MHz, frequencies of 5 MHz and higher are now the norm for clinical ultrasound imaging. At this frequency λ is ≈500μm in Araldite 2020, thus a particle size of 25 μm meets the criteria for Rayleigh scattering. There may be an additional advantage of using a larger particle size as no sieving of the powder was found necessary to prevent flocculation during mixing for any of the composites made. Anecdotally we are aware that other workers have sieved the tungsten powder before mixing to prevent flocculation although in many cases the particle size was very much smaller than the 25 μm particle size we used, in some cases as small as 1 μm. In terms of the original stimulus for the work reported in this paper, it should also be noted that larger particle size tungsten powders are cheaper and more widely available than smaller particle sized powders.

The results presented in this paper, when taken with the modelling results reported previously [3] suggest that it is possible to construct a multi-element ultrasound transducer for a medical imaging system using craft-based techniques in resource poor environments. 3D printing technology allows housings to be produced to a standard design, with a much lower material cost, typically one-third. In addition, manufacture currently takes 4 h compared to several days for skilled machinists who exist in some, but not all, resource poor environments. Having the transducer is only part of the solution to having an imaging system for such environments: high speed data acquisition and processing instrumentation, including microcode, will also be required. The increasing availability of cheap, readily available single board high performance processors primarily intended for the hobby and education markets (e.g. www.pjrc.com), offer the potential for a multi-processor solution which is both affordable and maintainable. Such an imaging device has the potential to deliver the identified benefits of having diagnostic ultrasound in resource poor environments [1] whilst directly addressing at least some of the problems identified in achieving this [2].

Funding

RWT received support from the Undergraduate Research Support Scheme (URSS) funded through the University of Warwick's Materials Global Research Priority (GRP) initiative. This research did not receive any other specific grant from funding agencies in the public, commercial or not-for-profit sectors.

Ethical approval

Not required.

CRediT authorship contribution statement

A.J. Wilson: Conceptualization, Funding acquisition, Formal analysis, Investigation, Writing – original draft. **R.W. Taylor:** Investigation. **S.E. Burrows:** Investigation, Supervision. **S.M. Dixon:** Funding acquisition, Supervision, Project administration.

Declaration of competing interest

None Declared

Acknowledgments

The support of Jim Dimond, Consultant Prosthetist, and his colleagues in the maxillofacial prosthetics laboratory at the University Hospital in Coventry who produced the 3D-prints using the photopolymer resins is gratefully acknowledged.

References

[1] S. Sippel, k. Muruganandan, A. Levine, S. Shah, Use of ultrasound in the developing world, Int. J. Emerg. Med. 4 (2011) 72.
[2] S. Shah, B. Bellows, S. Sippel, A. Adedipe, J. Totten, B. Backlund, D. Sajed, Perceived barriers in the use of ultrasound in developing countries, Crit. Ultrasound J. 7 (2015) 11.
[3] A. Wilson, Towards using a focussed phased array of millimetre length scale elements for ultrasound imaging, Phys. Med. Biol. 63 (14) (2018) 45009.
[4] A. Aitkenhead, J. Mills, A. Wilson, The design and characterisation of an ultrasound phased array suitable for deep tissue hyperthermia, Ultrasound Med. Biol. 34 (11) (2008) 1793–1807.
[5] C. Hill, Generation and structure of acoustic fields, Hill, C., Bamber, J., ter Haar G. (eds.), in: Medical Ultrasonics, Chichster, UK, John Wiley and Sons Ltd., 1998, pp. 41–68.
[6] C. Desilets, J. Fraser, G. King, The design of efficient broad-band piezoelectric transducers, IEEE Trans. Sonics Ultrason. SU-25 (1978) 115–125.
[7] C. Sayers, C. Tait, Ultrasonic properties of transducer backings, Ultrasonics 23 (2) (1984) 57–60.
[8] Araldite 2020 data sheet. Huntsman advanced materials, Basal Switzerland. 2007.
[9] H. Lamb, Hydrodynamics, 6th ed., 337, The University Press, Cambridge, 1932, p. p599.